Pergamon

Int. J. Solids Structures Vol. 31, No. 18, pp. 2445–2461, 1994

0020–7683/94 $7.00 + .00

0020–7683(94)E0050–6

INCIPIENT SEPARATION BETWEEN A FRICTIONLESS FLAT PUNCH AND AN ANISOTROPIC MULTILAYERED HALF PLANE

EDWARD E. URQUHART and MAREK-JERZY PINDERA
Civil Engineering and Applied Mechanics, University of Virginia, Charlottesville, Virginia, U.S.A.

(*Received* 9 *August* 1993; *in revised form* 20 *March* 1994)

Abstract—A solution to the frictionless contact of rigid flat indenters on arbitrarily layered, anisotropic half planes is obtained using Fourier transforms and the local–global stiffness matrix technique. The local–global stiffness matrix method involves reformulating the problem in terms of interfacial displacements as the basic unknowns, and has been shown to be an efficient method for solving mixed boundary-value problems of laminated media. The contact problem of a rigid punch gives rise to a mixed boundary condition of known displacement gradient and unknown pressure distribution in the contact area. This mixed boundary condition is reduced to a singular integral equation involving the unknown pressure using the asymptotic properties of the global stiffness matrix. A solution for the contact pressure distribution is then obtained from the singular integral equation using a technique provided by Erdogan, which involves the use of orthogonal Chebychev polynomials. The results are employed to determine the boundaries between full and two-region, and full and three-region, contact solution zones in separation parameter spaces that illustrate the effect of geometric and material parameters on the incipient separation between a flat punch and the top layer of a half plane laminated with isotropic, transversely isotropic and monoclinic plies.

INTRODUCTION

Frictionless contact problems of layered media have been studied extensively within the framework of linear elasticity. Recently, an efficient method of solving this class of mixed boundary-value problems has been developed. The local–global stiffness matrix method, employed by Pindera (1991) and Pindera and Lane (1993a,b) to solve round punch contact problems of arbitrarily laminated media, is based on a flexibility matrix approach outlined by Bufler (1971). Rowe and Booker (1982) later reformulated this approach in terms of local stiffness matrices and applied it to non-homogeneous isotropic layered media. Chatterjee *et al.* (1982) and Chatterjee (1987), used the method to solve interlaminar crack problems in anisotropic layered media. Most recently, Binienda and Pindera (1994) employed this technique to discuss differences and similarities in the response of metal matrix and polymeric matrix composite half planes indented by frictionless parabolic punches.

The frictionless contact problem is typically reduced to a singular integral equation for the unknown pressure distribution in the contact region using the surface mixed boundary conditions involving zero tractions outside the contact region and the constraint on the surface displacement provided by the punch profile inside this region. The solution for the unknown pressure distribution requires separation of the kernel in the integral equation into singular and regular parts. As discussed by Pindera and Lane (1993a), the local–global stiffness matrix approach naturally facilitates decomposition of the integral equation into singular and regular parts for an arbitrarily layered half plane comprising any number of layers. This decomposition utilizes the asymptotic behavior of the local, and thus global, stiffness matrix in the Fourier transform domain and a relation between Fourier and finite Hilbert transforms of the contact pressure. The resulting singular integral equation possesses a Cauchy-type kernel and is amenable to treatment by a collocation technique based on the properties of orthogonal polynomials outlined by Erdogan (1969) and Erdogan and Gupta (1972).

In this paper the authors briefly outline the development of the local–global stiffness matrix method, and show how it can be applied to study the contact response of a flat punch on an anisotropic layered half plane. The solution for the contact pressure predicts

complete contact between the punch and the half plane for only a limited range of geometric and material parameters. Outside this range separation occurs in either one or two areas of the contact region. This local separation phenomenon was first investigated by Shield and Bogy (1989) for isotropic configurations using a transform matrix technique. Here a generalized plane deformation formulation is employed which allows separation to be studied with regard to configurations consisting of anisotropic composite plies. The focus of this paper is the effect of off-axis ply orientation and material property mismatch between the composite plies and the supporting half plane on the boundaries between full and two-region, and full and three-region, contact solution zones in separation parameter spaces. The separation parameter spaces illustrate the effect of fiber volume fraction, fiber orientation and geometry on the incipient separation phenomenon.

PROBLEM FORMULATION

The laminated half plane shown in Fig. 1 consists of an arbitrary number of discrete layers bonded to a homogeneous supporting half plane, and is indented by a rigid flat punch. The half plane can be laminated with any combination of different materials arranged in any stacking order. Isotropic, orthotropic and off-axis (monoclinic) layers are admitted in the formulation. Inclusion of monoclinic materials renders the model ideally suited for the analysis of off-axis fibrous composites. The layers are numbered from $k = 1$ to n, where 1 and n designate the top layer and the homogeneous supporting half plane, respectively. Local Cartesian coordinate systems (x–y–z), are centered in the midplanes of the layers with the z-axis directed opposite to the applied load. By definition, the layers extend to infinity in the x–y plane. Expressions are developed which relate the stresses on the top and bottom of the individual plies to the corresponding displacements, and are grouped into local stiffness matrices. These local stiffness matrices are then assembled into a global stiffness matrix using interfacial continuity of tractions and displacements.

The displacement formulation of linear elasticity is employed and generalized plane deformation is assumed, where the three displacement components, u, v and w, are functions of only the x and z coordinates. Combining constitutive relations and the strain–displacement equations with the equations of equilibrium provides the Navier equations, which govern the functional form of the three displacement components. For a monoclinic layer these three partial differential equations are coupled in u, v and w, and have the following form,

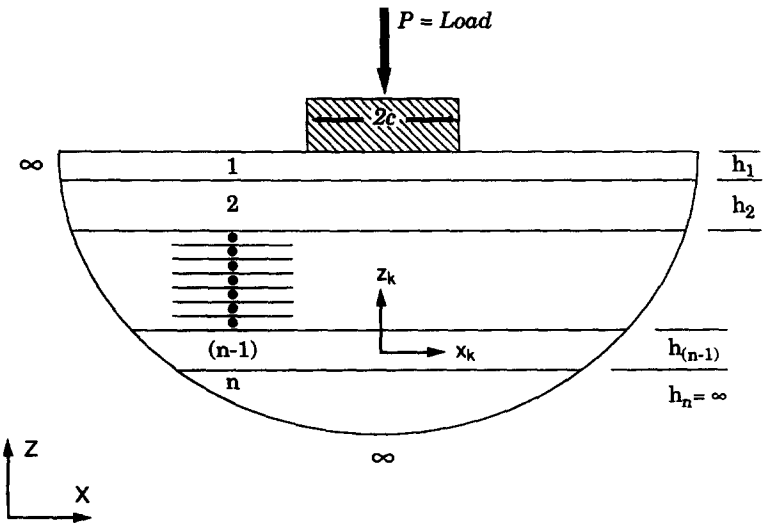

Fig. 1. Arbitrarily laminated half plane constructed with isotropic, transversely isotropic or monoclinic layers.

$$\bar{C}_{11}\frac{\partial^2 u}{\partial x^2}+\bar{C}_{55}\frac{\partial^2 u}{\partial z^2}+\bar{C}_{16}\frac{\partial^2 v}{\partial x^2}+\bar{C}_{45}\frac{\partial^2 v}{\partial z^2}+(\bar{C}_{13}+\bar{C}_{55})\frac{\partial^2 w}{\partial x\,\partial z}=0$$

$$\bar{C}_{16}\frac{\partial^2 u}{\partial x^2}+\bar{C}_{45}\frac{\partial^2 u}{\partial z^2}+\bar{C}_{66}\frac{\partial^2 v}{\partial x^2}+\bar{C}_{44}\frac{\partial^2 v}{\partial z^2}+(\bar{C}_{36}+\bar{C}_{45})\frac{\partial^2 w}{\partial x\,\partial z}=0$$

$$(\bar{C}_{13}+\bar{C}_{55})\frac{\partial^2 u}{\partial x\,\partial z}+(\bar{C}_{36}+\bar{C}_{45})\frac{\partial^2 v}{\partial x\,\partial z}+\bar{C}_{55}\frac{\partial^2 w}{\partial x^2}+\bar{C}_{33}\frac{\partial^2 w}{\partial z^2}=0 \tag{1}$$

where $\bar{C}_{ij}$s are the elements of the elastic stiffness matrix referred to the global coordinate system. The governing equations for orthotropic and isotropic layers have similar form but are uncoupled in the y-direction and can be obtained from eqn (1) by setting $C_{16}=C_{45}=C_{36}=0$. These governing differential equations are solved for each individual layer subject to the appropriate boundary conditions. Due to indentation by the flat punch, the top layer is subject to mixed boundary conditions. The displacement gradient in the contact region is governed by the profile of the punch, the tractions outside the contact region are required to vanish, and because the contact is assumed frictionless, there are no shear traction components on the top surface,

$$\begin{aligned}\frac{\mathrm{d}}{\mathrm{d}x}w_1(x,+h_1/2)&=0 \quad |x|<c\\ \sigma_{zz}&=0 \quad |x|>c\\ \sigma_{xz}=\sigma_{yz}&=0 \quad |x|\geqslant 0.\end{aligned} \tag{2}$$

The individual laminae of the composite structure in Fig. 1 are assumed firmly bonded together with no separations. Therefore, the traction and displacement components across the interface between two adjacent layers are continuous,

$$\begin{aligned}\mathbf{u}^k(x,-h_k/2)&=\mathbf{u}^{k+1}(x,h_{k+1}/2) \quad i=x,y,z\\ \sigma_{iz}^k(x,-h_k/2)&=\sigma_{iz}^{k+1}(x,h_{k+1}/2) \quad k=1,\ldots,n\end{aligned} \tag{3}$$

where k designates the layer number, $\mathbf{u}^k=(w_k,u_k,v_k)$ is a vector of interfacial displacements, and $\sigma_{iz}^k=(\sigma_{zz}^k,\sigma_{xz}^k,\sigma_{yz}^k)$ is a vector of interfacial tractions.

The solutions to the governing equations provide expressions for displacements throughout the individual layers. To obtain these solutions, infinite Fourier transforms are applied to reduce the partial differential equations to ordinary differential equations that are functions of z and the transform variable s. The transformed ordinary differential equations are subsequently solved using standard techniques.

SOLUTIONS FOR MULTILAYERED MEDIA

The solution of the governing differential equations in the transform domain provides the functional form of the displacement field in a given layer in terms of Fourier coefficients. Differentiation and application of constitutive law subsequently provides the functional form of the stress field (also in terms of Fourier coefficients). Expressions for displacement and stress components have been provided by Urquhart (1993). The problem is then reformulated by algebraically expressing interfacial tractions in terms of interfacial displacements, thereby eliminating the Fourier coefficients and constructing a local stiffness matrix for a given layer. A local stiffness matrix for a monoclinic layer has the form,

$$\begin{Bmatrix} \bar{\sigma}_{zz}^{+}/\mathrm{i}s \\ \bar{\sigma}_{xz}^{+}/s \\ \bar{\sigma}_{yz}^{+}/s \\ -\bar{\sigma}_{zz}^{-}/\mathrm{i}s \\ -\bar{\sigma}_{xz}^{-}/s \\ -\bar{\sigma}_{yz}^{-}/s \end{Bmatrix} = \begin{bmatrix} k_{11} & k_{12} & k_{13} & k_{14} & k_{15} & k_{16} \\ & k_{22} & k_{23} & k_{24} & k_{25} & k_{26} \\ & & k_{33} & k_{34} & k_{35} & k_{36} \\ & & & k_{44} & k_{45} & k_{46} \\ \text{SYM} & & & & k_{55} & k_{56} \\ & & & & & k_{66} \end{bmatrix} \begin{Bmatrix} \bar{w}^{+}/\mathrm{i} \\ \bar{u}^{+} \\ \bar{v}^{+} \\ \bar{w}^{-}/\mathrm{i} \\ \bar{u}^{-} \\ \bar{v}^{-} \end{Bmatrix} \tag{4}$$

where the "+" and "−" superscripts refer to the top and bottom of the layer, respectively. The elements k_{ij} for isotropic, orthotropic and monoclinic laminae have been provided by Pindera (1991), and are functions of a layer's material properties, thickness and the Fourier transform parameter s. In the case of an orthotropic or isotropic layer, the elements k_{13} $k_{16}, k_{23}, k_{26}, k_{34}, k_{35}, k_{46}$ and k_{56} vanish. Having determined the local stiffness matrices for each layer, a global stiffness matrix is assembled by observing interfacial continuity and boundary conditions. This assembly process is facilitated by rewriting eqn (4) in symbolic form as follows,

$$\begin{bmatrix} K_{11}^{k} & K_{12}^{k} \\ K_{21}^{k} & K_{22}^{k} \end{bmatrix} \begin{bmatrix} \bar{U}_{k}^{+} \\ \bar{U}_{k}^{-} \end{bmatrix} = \begin{bmatrix} \bar{T}_{k}^{+} \\ \bar{T}_{k}^{-} \end{bmatrix} \tag{5}$$

where $\bar{U}_{k}^{\pm}$ is the displacement vector on the surface of a ply, $\bar{T}_{k}^{\pm}$ is the corresponding traction vector divided by the Fourier transform parameter s, and the elements K_{ij}^{k} are 3×3 submatrices of the local stiffness matrix. The interfacial continuity conditions of eqn (3) require the sum of the tractions acting along the kth interface to be zero, i.e.

$$\bar{T}_{k}^{-} + \bar{T}_{k+1}^{+} = 0 \quad k = 1, \ldots, (n-1). \tag{6}$$

Equation (3) also ensures that the displacement on the bottom surface of a layer is equal to the displacement on the top surface of the layer directly underneath,

$$\bar{U}_{k}^{-} = \bar{U}_{k+1}^{+} = \bar{U}_{k+1} \quad k = 1, \ldots, (n-1). \tag{7}$$

The system of equations that comprises the global stiffness matrix is obtained by starting with the top surface, where the unknown traction in the contact region is represented by $\bar{T}_{1}^{+}$, and then applying eqn (6) to each interface using eqn (7) to eliminate redundant interfacial displacement terms (eliminate the $\bar{U}_{k}^{-}$ terms),

$$\begin{aligned} \text{top layer:} \quad & \bar{T}_{1}^{+} = \bar{K}_{11}^{1}\bar{U}_{1} + \bar{K}_{12}^{1}\bar{U}_{2} \\ k\text{th interface:} \quad & 0 = \bar{K}_{21}^{k}\bar{U}_{k} + (\bar{K}_{22}^{k} + \bar{K}_{11}^{k+1})\bar{U}_{k+1} + \bar{K}_{12}^{k+1}\bar{U}_{k+2} \\ \text{supporting half plane:} \quad & 0 = \bar{K}_{21}^{n-1}U_{n-1} + (\bar{K}_{22}^{n-1} + \bar{K}_{11}^{*n})\bar{U}_{n} \end{aligned} \tag{8}$$

where n is the total number of layers including the half plane and K_{11}^{*n} is the local stiffness matrix for the supporting half plane. The elements of the local stiffness matrices for half planes also have been provided by Pindera (1991). The assembly of the global stiffness matrix for the entire layered medium is carried out, according to eqn (8), by superposing individual local stiffness matrices along the main diagonal of the global stiffness matrix in an overlapping fashion,

$$\begin{bmatrix} K_{11}^1 & K_{12}^1 & 0 & \cdot & \cdot \\ K_{21}^1 & (K_{22}^1+K_{11}^2) & K_{12}^1 & \cdot & \cdot \\ 0 & K_{21}^2 & (K_{22}^2+K_{11}^3) & \cdot & \cdot \\ 0 & 0 & K_{21}^3 & \cdot & \cdot \\ 0 & \cdot & \cdot & \cdot & (K_{22}^{n-1}+K_{11}^{*n}) \end{bmatrix} \begin{bmatrix} \bar{U}_1 \\ \bar{U}_2 \\ \cdot \\ \cdot \\ \bar{U}_n \end{bmatrix} = \begin{bmatrix} \bar{T}_1^+ \\ 0 \\ \cdot \\ \cdot \\ 0 \end{bmatrix}. \tag{9}$$

Since continuity of interfacial displacements is enforced directly through eqn (7), the above procedure results in a reduction in the number of unknowns through elimination of the redundant continuity equations that are retained in the standard approach. In configurations with many layers, formulating the problem in terms of a global stiffness matrix results in almost a 50% reduction in the number of unknowns, thus substantially reducing subsequent computational effort.

FORMULATION AND SOLUTION OF THE SINGULAR INTEGRAL EQUATION

By inverting the global stiffness matrix, the interfacial displacements are related to the applied tractions, and since the only traction component is the normal contact pressure on the top surface,

$$\begin{Bmatrix} \bar{w}^1/\mathrm{i} \\ \bar{u}^1 \\ \bar{v}^1 \\ \bullet \end{Bmatrix} = \begin{bmatrix} H_{11} & H_{12} & H_{13} & \bullet \\ H_{12} & H_{22} & H_{23} & \bullet \\ H_{13} & H_{23} & H_{33} & \bullet \\ \bullet & \bullet & \bullet & \bullet \end{bmatrix} \begin{Bmatrix} \bar{\sigma}_{zz}^1/\mathrm{i}s \\ 0 \\ 0 \\ \bullet \end{Bmatrix} \tag{10}$$

where H_{ij} are the elements of the inverse of the global stiffness matrix in eqn (9). Consequently, the relationship between the normal displacement and the applied traction on the top surface involves only the H_{11} term,

$$\bar{w}_1(s) = H_{11}(s)\bar{\sigma}_{zz}^1(s)/s \tag{11}$$

where $\bar{\sigma}_{zz}^1(s)$ is the transform of the contact pressure, $p(t)$, given by,

$$\bar{\sigma}_{zz}^1(s) = \frac{1}{\sqrt{2\pi}} \int_{-c}^{c} p(t)\, \mathrm{e}^{\mathrm{i}st}\, \mathrm{d}t = \bar{p}(s). \tag{12}$$

Imposing the displacement boundary condition, eqn (2), over the contact region we obtain an integral equation involving the unknown contact pressure $p(t)$,

$$\frac{\mathrm{d}}{\mathrm{d}x} w_1 = \frac{-\mathrm{i}}{\sqrt{2\pi}} \int_{-\infty}^{+\infty} s\bar{w}_1\, \mathrm{e}^{-\mathrm{i}sx}\, \mathrm{d}s = \frac{-\mathrm{i}}{2\pi} \int_{-\infty}^{+\infty} H_{11}(s) \left[\int_{-c}^{c} p(t)\, \mathrm{e}^{\mathrm{i}st}\, \mathrm{d}t \right] \mathrm{e}^{-\mathrm{i}sx}\, \mathrm{d}s = 0. \tag{13}$$

The above integral equation is singular because as s approaches infinity, $H_{11}(s)$ does not vanish. The singular nature of the kernel can be identified by considering the asymptotic behavior of the local, and thus global, stiffness matrix for large values of s. In this case, the elements of the local stiffness matrix relating the tractions and displacements on the top surface of a layer become uncoupled from those on the bottom,

$$\begin{bmatrix} K_{11}^{*k} & 0 \\ 0 & K_{22}^{*k} \end{bmatrix} \begin{bmatrix} \bar{U}_k^+ \\ \bar{U}_k^- \end{bmatrix} = \begin{bmatrix} \bar{T}_k^+ \\ \bar{T}_k^- \end{bmatrix} \tag{14}$$

where the elements of the submatrices K_{11}^{*k} and K_{22}^{*k} depend only on material properties of the layer and the sign of the transform variable s (Pindera and Lane, 1993a). The elements of the submatrix K_{11}^{*k} are precisely the same as the corresponding elements for the local stiffness matrix of a homogeneous half plane having the same elastic properties as those of a given layer. The limiting behavior of the kernel $H_{11}(s)$ is thus

$$\lim_{s \to \pm\infty} H_{11}(s) = \operatorname{sgn}(s) H_{11}^{*} \tag{15}$$

where $\operatorname{sgn}(s)\mathrm{H}_{11}^{*}$ is the first element of the inverse of the submatrix $[K_{11}^{*1}]$. Using eqn (15), the kernel $H_{11}(s)$ in eqn (13) is separated into singular and regular parts, $\operatorname{sgn}(s)H_{11}^{*}$ and $H_{11}^{0}(s) = H_{11}(s) - \operatorname{sgn}(s)H_{11}^{*}$, respectively, yielding

$$\frac{\mathrm{d}}{\mathrm{d}x} w_1 = \frac{-\mathrm{i}}{2\pi} \int_{-\infty}^{+\infty} (\operatorname{sgn}(s) H_{11}^{*} + H_{11}^{0}(s)) \left[\int_{-c}^{c} p(t)\, \mathrm{e}^{\mathrm{i}st}\, \mathrm{d}t \right] \mathrm{e}^{-\mathrm{i}sx}\, \mathrm{d}s. \tag{16}$$

The asymptotic form of the local stiffness matrix, eqn (14), reveals that the asymptotic relation between the transformed displacements and tractions on the surface of a layered half plane is the same as that obtained for a homogeneous half plane having the properties of the surface layer. In view of this, a relation between the Fourier and finite Hilbert transforms of the contact pressure can be derived by considering $\lim_{z \to 0} [(\partial/\partial x) w(x, z)]$ of the homogeneous half plane problem (Gladwell, 1980, p. 210),

$$\frac{-\mathrm{i}}{\sqrt{2\pi}} \int_{-\infty}^{+\infty} \operatorname{sgn}(s) \bar{p}(s)\, \mathrm{e}^{-\mathrm{i}sx}\, \mathrm{d}s = \frac{1}{\pi} \int_{-c}^{c} \frac{p(t)}{t-x}\, \mathrm{d}t \tag{17}$$

reducing the dominant part of the singular integral in eqn (16) to an integral containing a Cauchy kernel. Using the odd–even properties of the regular kernel, integration limits may be changed and the following form of eqn (16) is obtained:

$$\frac{\mathrm{d}}{\mathrm{d}x} w_1 = \frac{H_{11}^{*}}{\pi} \int_{-c}^{c} \frac{p(t)}{t-x}\, \mathrm{d}t + \frac{1}{\pi} \int_{0}^{+\infty} \int_{-c}^{c} H_{11}^{0}(s) p(t) \sin(t-x)s\, \mathrm{d}t\, \mathrm{d}s. \tag{18}$$

A numerical collocation technique to solve singular integral equations of the above form has been developed by Erdogan (1969) and Erdogan and Gupta (1972). The method assumes that the unknown function (in this case the contact pressure) can be expanded in a series of orthogonal polynomials which are multiplied by a suitable weight function. The choice of the appropriate polynomials is determined by the nature of the singularities and the form of the weight function is determined by the characteristic distribution of the contact pressure. For flat punch contact problems, Chebychev polynomials of the first kind are used.

The polynomials are of order n, where each term is multiplied by an influence coefficient. Since the polynomials are defined on an interval between plus and minus one, suitable normalization must be applied to the contact dimension. To determine the n unknowns generated by the polynomial approximation, the contact region is divided into $n+1$ discrete intervals and a system of linear equations involving the kernel of the integrand and the known displacement gradients is assembled. A Gauss quadrature integration scheme is employed to evaluate the kernels. If the order of the integrator is greater than or equal to n, and the location of the integration points coincides with the zeros of the orthogonal polynomials, the integration is exact. Once the kernels are evaluated, the system

of equations is numerically inverted to obtain the influence coefficients, and thus the pressures at the n collocation points. The accuracy of the approximation is limited only by the number of collocation points used. The contact pressure, $p(x)$, is approximated by,

$$p(x) = \frac{F(x)}{\sqrt{1-x^2}}, \quad F(x) = \sum_{i=0}^{n} B_i T_i(x), \quad T_i(x) = \cos(i\theta), \cos\theta = x \tag{19}$$

where $T_i(x)$ is a Chebychev polynomial of the first kind, $1/\sqrt{1-x^2}$ is the associated weight function, and the B_is are the unknown influence coefficients. Consequently, Erdogan shows that eqn (18) can be reduced to the following system of linear equations,

$$\sum_{k=1}^{n} \frac{1}{n} F(t_k) \left[\frac{1}{t_k - x_r} + \pi K_0(x_r, t_k) \right] = f(x_r) \quad r = 1, \ldots, n-1 \tag{20}$$

where

$$t_k = \cos\left[\frac{\pi}{2n}(2k-1)\right], \quad x_r = \cos\left[\frac{\pi r}{n}\right]$$

and the inhomogeneous term is given by the slope of the punch, $f(x_r) = (\mathrm{d}/\mathrm{d}x)w_1(x_r)/H_{11}^*$, which for a flat punch is zero. The regular kernel $K_0(x_r, t_k)$ in eqn (20),

$$K_0(x, t) = \frac{1}{\pi} \int_0^\infty \frac{H_{11}^0(s)}{H_{11}^*} \sin(t-x)s \, \mathrm{d}s$$

is symmetric with respect to $r = n/2$, and is therefore evaluated only from $r = 1$ to $(n/2)$. However, the system of equations represented by eqn (20) involves only $(n-1)$ equations for n unknowns, therefore an additional equation is needed. The final equation comes from the load condition, where the pressure under the punch must integrate to give the total applied load,

$$\sum_{k=1}^{n} \frac{\pi}{n} F(t_k) = P = \text{Load}. \tag{21}$$

Solution of the system of equations given by eqns (20) and (21) provides the unknown values of $F(t)$ at the collocation points t_k in eqn (19) which are needed to determine the unknown pressure distribution in the contact region.

NUMERICAL INTEGRATION OF THE KERNEL $K_0(x_r, t_k)$

The most time-consuming aspect of solving the system of equations formed by eqns (20) and (21) is the calculation of the kernel $K_0(x_r, t_k)$, since it involves an "infinite" integration with respect to the transform variable s. Considerable effort has gone into improving the numerical efficiency of this integration, which is based on the original algorithm developed by Pindera (1991). The calculation of $K_0(x_r, t_k)$ involves only two terms from the global stiffness matrix, namely $H_{11}(s)$ and its asymptotic limit H_{11}^*. All material and geometric features of a configuration are completely characterized by these two terms. $H_{11}(s)$ is obtained by inverting the global stiffness matrix at every value of s throughout the integration interval, whereas H_{11}^* is independent of the transform variable and is obtained from the inverse of the submatrix $[K_{11}^{*1}]$, which obviously is carried out just once.

The kernel $K_0(x_r, t_k)$ can be viewed as a combination of two terms. The first term, $\sin(t_k - x_r)s$, is periodic with the period $2\pi/(t_k - x_r)$, where t_k and x_r are given by eqn (20).

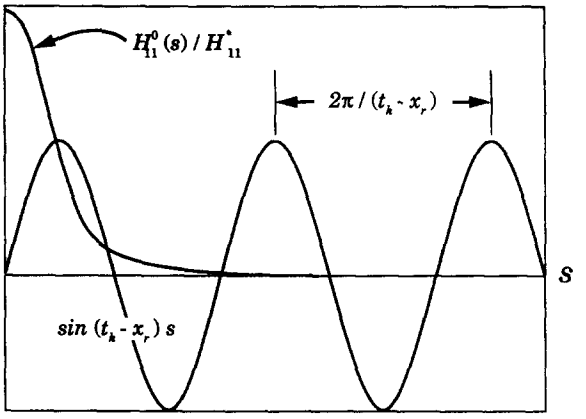

Fig. 2. Typical examples of the sinusoidal and decaying terms in the integrand of K_0.

The second term, $H_{11}^0(s)/H_{11}^*$, has a functional form and a convergence rate (with respect to s) that depend on the geometry and material configuration of the half plane. Figure 2 illustrates typical examples of both terms. The two terms depicted in Fig. 2 combine to produce a kernel which oscillates as it converges. The kernel must be evaluated for every distinct combination of t_k and x_r, with r ranging from 1 to $(n/2+1)$, and k ranging from 1 to n, where n is the number of collocation points. This represents $(n^2/2+n)$ integrations over the s domain. The integration is performed by dividing the integrands into increments of variable length, and using Gauss quadrature on each interval. By appropriately selecting the width of each integration interval to coincide with the "zero's" of the oscillation, the accuracy and efficiency of the integration is greatly improved.

The sinusoidal terms in the integrands of the kernels have different periods, depending on the values of k and r. Certain combinations of k and r produce a high frequency of oscillation, requiring a small integration interval, while others combine to produce a low frequency. The rate of convergence of the kernel depends mainly on the $H_{11}^0(s)/H_{11}^*$ term, therefore the individual kernels are integrated simultaneously and truncated at the same value of s. The Gaussian quadrature integration scheme is performed by mapping the individual integration intervals onto the interval $[-1, +1]$, using the following transformation of the variable s,

$$2s = (b+a)+(b-a)s_d$$

where a and b are the lower and upper limits of integration, respectively. Once the function has been mapped onto the new interval, it is evaluated at a number of locations (depending on the accuracy desired) given by s_d, and multiplied by the corresponding Gauss weight factor. Values of s_d and their corresponding weights can be obtained from tables in various references (Abramowitz and Stegun, 1965). The value of the kernel (between the limits of a and b) is then obtained by summing the individual contributions. This process is repeated, incrementing a and b, until K_0 converges.

Since the integration intervals are variable (depending on k and r), the locations of the s_ds in each interval are different, requiring the integrand to be evaluated numerous times for different combinations of k and r. If a 64 point integration scheme is used, a single integration period requires the kernel to be evaluated at $64\bullet(n^2/2+n)$ locations, and often thousands of integration intervals are required to achieve convergence. Evaluating the term $H_{11}(s)$ (appearing in the integrand) requires developing "s-dependent" local stiffness matrices, assembling them into a global stiffness matrix, inverting the global stiffness matrix, and extracting its (1, 1) element. For configurations having many layers this process is numerically intensive.

To avoid having to calculate $H_{11}(s)$ repeatedly, a cubic spline interpolation routine is employed. The function $H_{11}(s)$ is evaluated along s at evenly spaced intervals, and the slope of the function is then calculated between the intervals. If the slope is too large between

any two points (i.e. the function is changing rapidly), the interval is further divided and $H_{11}(s)$ and its slopes are calculated at the new subdivisions. The discrete values and slopes are stored in arrays to be used by an interpolation subroutine. Thus, the values of $H_{11}(s)$ are determined for any s simply by invoking the subroutine. Using an interpolation routine, the kernel is evaluated by calculating $H_{11}(s)$ a few hundred times, as opposed to thousands (even hundreds of thousands) of times when evaluated directly. Because $H_{11}(s)$ is a relatively smooth function, there is virtually no loss of accuracy in using the interpolation routine. The kernel is continuously monitored throughout the integration, and truncated only if a "small" change in its value is observed after a complete cycle of integration. The algorithm used to implement the integration of the kernels is described in more detail in Urquhart (1993).

PREDICTING SEPARATION

When a flat punch indents a layered half plane in the absence of friction and surface bonding, there is no physical mechanism to ensure that the punch remains in full contact with the half plane. Full contact occurs only for a limited range of geometric and material parameters. Outside of this range, certain combinations of parameters lead to regions of separation between the punch and the half plane. Separation will occur if the normal stress between the punch and the half plane predicted by the solution is tensile at any point in the contact region, since there is no bonding agent to ensure contact. Separation can occur in either one or two regions of the contact area (Shield and Bogy, 1989). If separation occurs in one region, the contact is referred to as "two-region" contact because there are two regions of positive contact between the punch and half plane. Similarly, separation in two regions is referred to as "three-region" contact.

The physical quantities of interest in a flat punch contact problem are the contact pressure distribution, and the separation parameter space. The parameter space illustrates the combinations of various physical parameters that form boundaries between full, two-region and three-region contact solutions. The parameter space is constructed by using an iterative bisectional root finding algorithm that solves eqn (18) for the contact pressure with respect to variations in material and geometric parameters (Urquhart, 1993). For a configuration with a given combination of physical parameters, eqn (18) is solved and the form of the contact pressure profile is examined to determine the nature of the contact (full, two- or three-region). The root finder continues to adjust the physical parameters until the boundaries of the separation parameter space are found. The present formulation is limited to the determination of separation boundaries between full and two-region, and full and three-region contact solutions. The third boundary between two-region and three-region contact solutions considered by Shield and Bogy for isotropic layered half planes will be considered at a later time.

There are two non-dimensional parameters that affect separation in isotropic configurations as discussed by Shield and Bogy (1989). The geometric parameter α is the ratio of the punch half-width to the height of the surface layer (or layers) bonded to the half plane (i.e. $\alpha = c/h$). The material parameter β is the ratio of the equivalent elastic modulus of the top layer (or layers) to that of the half plane (i.e. $\beta = E_1/E_h$). In anisotropic configurations, however, separation cannot be characterized by a single material parameter. However, one physically significant material parameter that affects separation in anisotropic fibrous composites is the fiber volume fraction, v_f. In anisotropic configurations, therefore, a parameter space is constructed by varying the fiber volume fraction in conjunction with any geometric parameters, and using a micromechanical model to calculate the equivalent material properties of the individual layers prior to solving eqn (18).

RESULTS

The effect of varying material and geometric parameters on the separation between a flat punch and a layered medium can best be illustrated by considering a configuration consisting of a single isotropic layer bonded to a homogeneous supporting half plane.

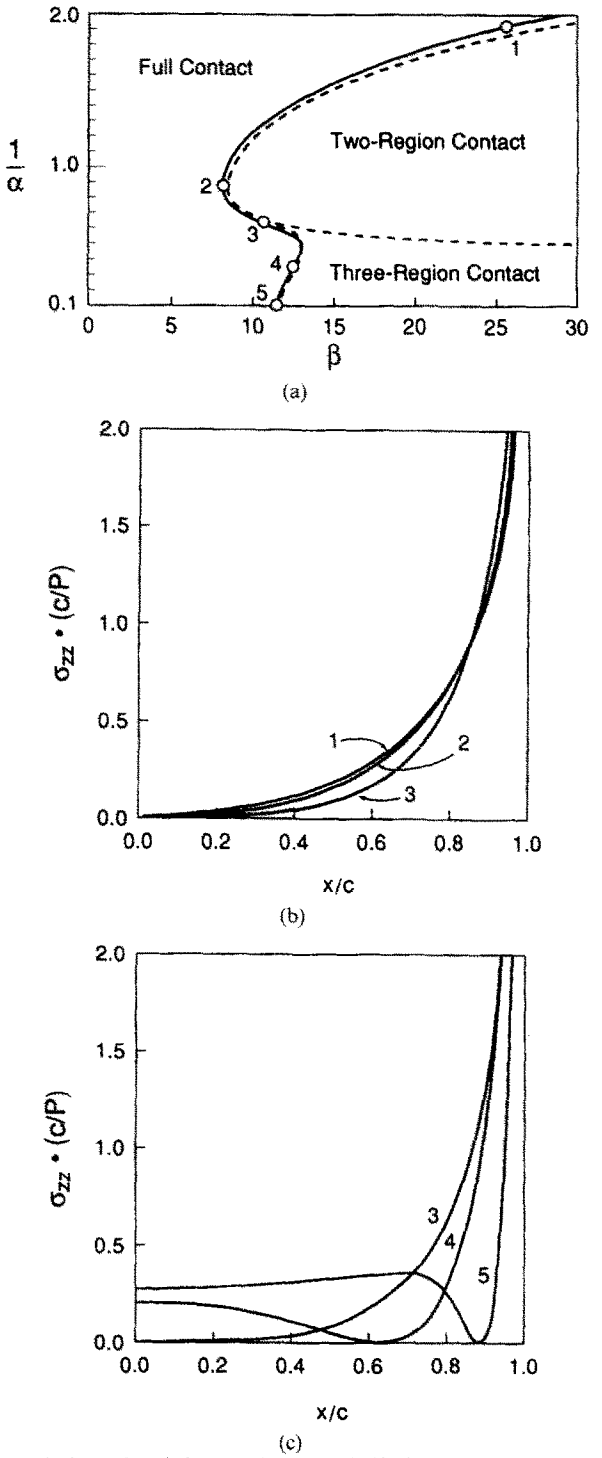

Fig. 3. Single isotropic layer bonded to an isotropic half plane: (a) separation space showing comparison between current analysis (——) and the results of Shield and Bogy (1989) (– – –); (b) pressure profiles corresponding to points 1, 2 and 3; (c) pressure profiles corresponding to points 3, 4 and 5.

Variations in the two parameters α and β result in deviations from the characteristic pressure profiles associated with each of the three types of contact mentioned above. Figure 3(a) illustrates the separation parameter space ($1/\alpha$ versus β) for such a configuration. The parameter space is compared with results obtained by Shield and Bogy (1989). The curves in the parameter space represent the combinations of parameters that separate the zones where full, two- and three-region contact is predicted. The intersection of these three lines

represents the unique combination where all three solutions exist simultaneously, and is designated the "triple point" (point 3) by Shield and Bogy (1989). Moving away from the triple point in the parameter space will result in either full, two- or three-region contact, depending on the direction travelled. The solution used by Shield and Bogy provides the boundary between the two- and three-region contact zones, whereas the method used in this study does not. The displacement boundary condition at the surface employed in our solution prescribes complete contact between the flat punch and the half plane. Therefore, the method used here allows contact pressure predictions only within the full contact zone, providing separation divisions from the full to two-, and from the full to three-region zones, but not from the two- to three-region zones. Comparing the results of the present analysis for the boundaries separating the full and two-region, and full and three-region contact solution spaces with those obtained by Shield and Bogy, it should be noted that the minor differences observed are most likely due to the different methods of numerical integration of the bounded part of the kernel in eqn (18). Both investigations arrive at the same governing equation for the contact pressure distribution, eqn (18), which is solved using the same polynomial expansion for the contact pressure and the solution technique of Erdogan and Gupta.

Figure 3(a) indicates that multiple region contact is predicted only in regions where β is significantly greater than one, indicating that separation in isotropic configurations occurs only when the surface layer is sufficiently stiffer than the substrate. Similarly, for the employed range of β, multiple region contact exists only when the $1/\alpha$ parameter is less than two, or when the width of the flat indenter is greater than the thickness of the surface layer.

Figures 3(b) and 3(c) illustrate pressure profiles generated with combinations of α and β that correspond to the five symbols shown in the parameter space of Fig. 3(a). These profiles were generated with 96 collocation points and normalized with respect to the applied load and the half-width c of the indenter, ensuring that $x/c = 1.0$ corresponds to the edge of the contact region and the corner of the punch. The profiles corresponding to the points 1–3 along the perimeter between the full and two-region contact solutions exhibit compressive stresses throughout the entire contact region, but are on the verge of becoming tensile in the center of the punch, implying a two-region contact solution. Similarly, the profiles corresponding to the points 3–5 along the perimeter between the full and three-region contact solutions are on the verge of predicting three-region contact. The profile corresponding to point 3 is generated with the unique combination of parameters given by the "triple point" and exhibits no stress at the center of the punch. Changing either α or β will alter this pressure distribution, and depending on how they are changed, either full, two or three-region contact will result.

In anisotropic configurations consisting of fiber-reinforced composite laminae, the orientation of an anisotropic lamina has a significant effect on the resulting contact pressure and separation parameter space due to the variations in the effective in-plane material properties that occur when a lamina is rotated through an angle in the plane perpendicular to the loading direction. The effect of off-axis orientation can best be illustrated by considering the configuration depicted in Fig. 4(a), consisting of a single graphite–epoxy lamina bonded to a homogeneous half plane. The separation space is constructed with respect to the two non-dimensional parameters, α and the fiber volume fraction v_f. The fiber volume fraction describes the volumetric ratio of fiber material to matrix material where $v_f = 0.0$ implies a homogeneous material consisting of matrix only, and $v_f = 1.0$ implies fiber material only. Both of these extremes ($v_f = 1.0$ and $v_f = 0.0$), may be physically impractical in a fibrous composite, however they represent a valid range of material parameters over which the contact pressure solution can be determined in an effort to study the separation phenomena. The material properties of a lamina increase with fiber volume fraction (assuming the stiffness of the fiber is greater than the matrix), hence the material property mismatch between the surface and the support increases with v_f as well. The micromechanics model called the method of cells is used to calculate the effective material properties of a lamina for a given fiber volume fraction (Aboudi, 1991). Material properties are given in Table 1 for the graphite fiber, the epoxy matrix and the isotropic foam half plane.

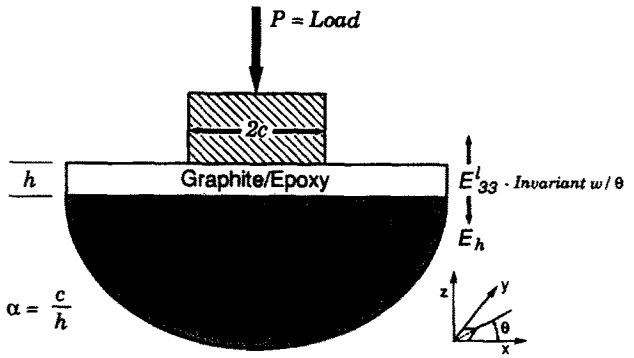

(a)

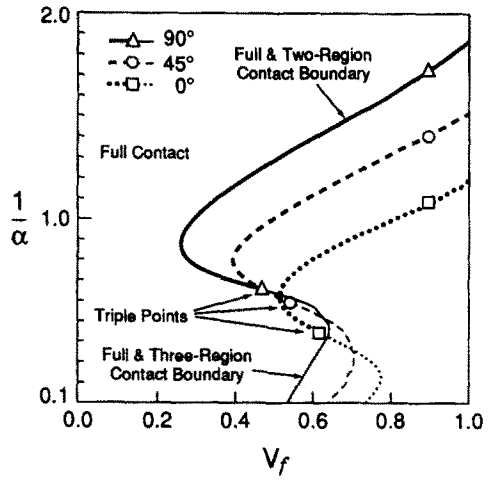

(b)

Fig. 4. (a) Single anisotropic layer bonded to a compliant isotropic half plane. (b) Separation parameter space showing the effects of ply orientation and fiber volume fraction on the boundaries between full and two-region, and full and three-region, contact solution zones.

Figure 4(b) depicts the separation parameter space for three separate ply orientations, 0, 45 and 90°. The solid, broken and dotted lines represent the boundaries between zones of full contact and two-region and three-region contact solutions for the three off-axis ply orientations, and the triple points for each case are given by the corresponding symbols. Since the ply orientation does not affect the through-the-thickness elastic modulus of the lamina, variations in the through-the-thickness elastic modulus mismatch between the surface layer and the supporting half plane are due solely to the fiber volume fraction

Table 1. Various fiber and matrix properties

Material	E_{11} (GPa)	E_{22} (GPa)	E_{33} (GPa)	G_{12} (GPa)	G_{13} (GPa)	G_{23} (GPa)	ν_{12}	ν_{13}	ν_{23}
Glass fiber	90.5	90.5	90.5	37.0	37.0	37.0	0.220	0.220	0.220
Graphite fiber	233.0	23.0	23.0	9.0	9.0	8.2	0.200	0.200	0.400
Boron fiber	400.0	400.0	400.0	166.8	166.8	166.8	0.200	0.200	0.200
SCS-6 SiC fiber	400.0	400.0	400.0	160.0	160.0	160.0	0.250	0.250	0.250
Epoxy matrix	5.35	5.35	5.35	1.98	1.98	1.98	0.350	0.350	0.350
Al-6061 matrix	72.4	72.4	72.4	27.2	27.2	27.2	0.333	0.333	0.333
Ti-6Al-4V matrix	110.0	110.0	110.0	42.0	42.0	42.0	0.310	0.310	0.310
Isotropic foam (Fig. 4)	0.862	0.862	0.862	0.324	0.324	0.324	0.330	0.330	0.330
Isotropic foam (Fig. 6)	9.05	9.05	9.05	3.39	3.39	3.39	0.333	0.333	0.333
Isotropic foam (Fig. 7)	0.110	0.110	0.110	0.045	0.045	0.045	0.230	0.230	0.230

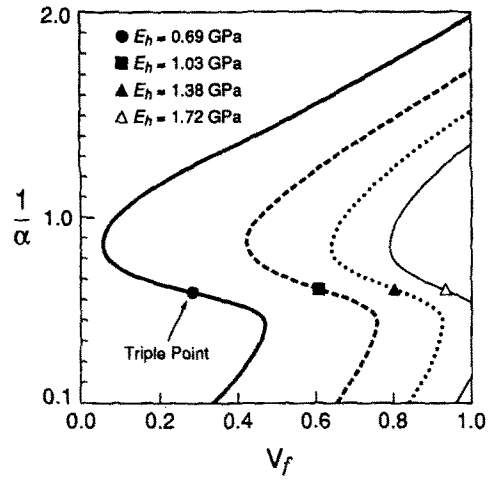

Fig. 5. Separation parameter space for a single 90° graphite–epoxy ply bonded to a compliant isotropic half plane showing the effects of different values of the half plane's Young's modulus and fiber content of the graphite–epoxy ply on the boundaries between full and two-region, and full and three-region, contact solution zones.

variation. The considerable difference between the three boundaries is a result of the variation in the in-plane material properties of the surface lamina brought about by rotating the lamina through the corresponding angles in the plane perpendicular to the loading direction. A lamina's resistance to local bending deformation is a function of the orientation of the fibers in the plane of the lamina. As a lamina bends under the application of load transferred through a flat punch, it tends to pull away or separate from the punch, pivoting on the corners. A 90° lamina offers the least amount of resistance to these local bending effects, and therefore a smaller fiber volume fraction (material property mismatch) is required to initiate separation. This condition is reflected by the relative shift between the three separation zones along the v_f-axis, and by the fact that the separation zones for the 90° lamina occupy a greater percentage of the parameter space than either the 0 or 45° cases.

The effect of varying the through-the-thickness material property mismatch is illustrated by considering two half plane configurations, both of which consist of a single anisotropic layer bonded to a homogeneous, isotropic supporting half plane. In the first configuration, a 90° surface lamina of graphite–epoxy is bonded to a homogeneous half plane whose elastic modulus is varied. Separation spaces are presented for various half plane moduli which range from 0.69 to 1.72 kPa (0.10–0.25 Msi). In the second case the supporting half plane modulus is fixed at 8.96 kPa (1.30 Msi), and three typical fibrous composite materials, glass–epoxy, boron–aluminum and silicon carbide–titanium, are used for the surface lamina. In both cases, the values of the half plane moduli were chosen so that separation would occur within the [0, 1] range of fiber volume fraction. The separation spaces for 0 and 90° surface laminae are presented for each configuration, with respect to the non-dimensional parameters $1/\alpha$ and v_f. The material properties of the constituents in the three composite material systems are included in Table 1.

Figure 5 illustrates the variations in separation space for a 90° graphite–epoxy lamina bonded to a homogeneous supporting half plane with an elastic modulus that is varied incrementally from 0.69 to 1.72 kPa (0.10–0.25 Msi). The moduli of the different supporting half planes are listed with their corresponding symbols. The location of the symbols in the separation space correspond to the "triple-points". The separation zone for the case $E_h = 0.69$ kPa (0.10 Msi) represents the configuration that is most susceptible to separation, as is evident by the percentage of area it occupies in the parameter space. The separation tendency is due to the large material property mismatch between the surface and substrate. As the modulus of the half plane is increased, the mismatch decreases along with the separation tendency, resulting in a right-hand shift in the separation curves.

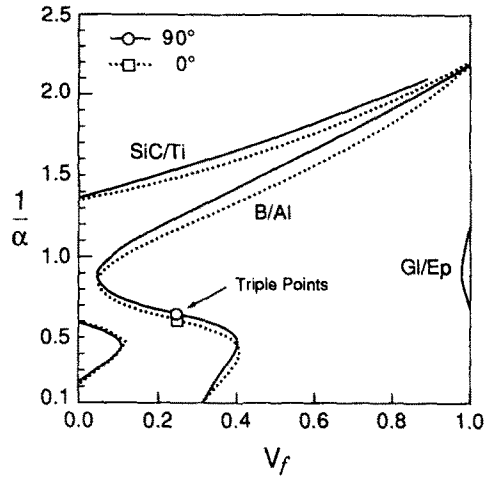

Fig. 6. Separation parameter space for glass–epoxy, boron–aluminum and silicon carbide–titanium plies bonded to a homogeneous half plane showing the effects of ply orientation and fiber content on the boundaries between full and two-region, and full and three-region, contact solution zones.

Figure 6 depicts the separation parameter spaces for glass–epoxy, boron–aluminum and silicon carbide–titanium laminae with 0 and 90° fiber orientations, bonded to an isotropic supporting half plane with a fixed elastic modulus, E_h, of 8.96 kPa (1.30 Msi). Only the 90° separation space is shown for glass–epoxy, because the 0° separation space lies outside the range of parameters. For this lamina, full contact is predicted for almost every combination of parameters, with the exception of a small separation zone near the right-hand side of the parameter space. The material properties of the glass–epoxy, especially through the thickness, are very near those of the half plane, resulting in the small separation zone.

The separation space for the boron–aluminum lamina bonded to the isotropic half plane is obtained for both 0 and 90° configurations. The triple points are given by the circular symbol for the 90° case and the square symbol for the 0° case. The area above the triple points and inside the separation zone corresponds to two-region separation, whereas the area below the triple points inside the separation zone corresponds to three-region separation. There is a small, but noticeable difference in the separation zones due to the fiber orientation, as would be expected. When the volume fraction is one or zero, the lamina is isotropic and the ply orientation has no effect on the contact pressure, therefore, the separation zones for the 0 and 90° lamina converge to the same $1/\alpha$ value. This does not occur for the graphite–epoxy lamina considered in Fig. 4(b). The reason for this is that the graphite fiber is transversely isotropic, and even though the material is homogeneous when $v_f = 1.0$ (all fiber), a rotation of the ply changes the in-plane material properties. Further, the through-the-thickness material property mismatch for the boron–aluminum lamina is significantly higher than that of the glass–epoxy case because the boron–aluminum has a larger through-the-thickness elastic modulus. Consequently, the separation zones are shifted to the left in the parameter space indicating a greater separation tendency. The separation zones occupy a large percentage of the area in the parameter space, whereas in the glass–epoxy configuration this percentage was exceedingly small.

The separation zones for the silicon carbide–titanium (SiC–Ti) lamina bonded to the isotropic half plane are also obtained for both 0 and 90° configurations. The triple points lie outside the parameter space and are not shown. The SiC–Ti lamina has the highest through-the-thickness modulus of the three materials considered, therefore, it also has the greatest separation tendency. This separation tendency is evident in the large percentage of the area occupied by the separation zones in the parameter space. Separation is predicted throughout the range of fiber volume fraction for much of the corresponding α range. If the elastic modulus of the half plane were decreased, the separation tendency would increase and the separation zones would shift to the left in the parameter space. In contrast, an

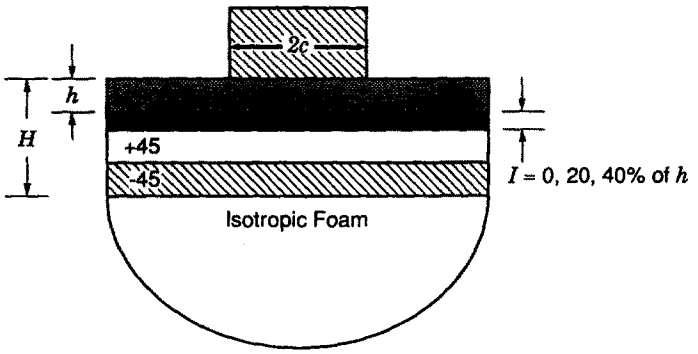

(a)

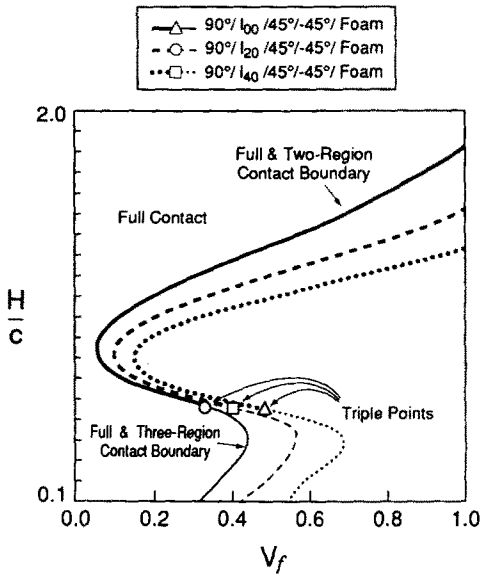

(b)

Fig. 7. (a) Laminated half plane geometry and stacking sequence for a $90°/I/\pm 45°$ graphite–epoxy laminate bonded to a homogeneous half plane. (b) Separation space showing the effects of a compliant subsurface layer's thickness and fiber content of the graphite–epoxy plies on the boundaries between full and two-region, and full and three-region, contact solution zones.

increase in the elastic modulus of the half plane would shift the separation zones to the right in the parameter space.

The last application of the outlined methodology focuses on multilayered composite laminates that are typically constructed by bonding together a number of laminae with various material properties and fiber orientations. The resulting laminate can exhibit effective material properties that differ from those of the individual plies. In the process of assembling the individual laminae, adhesives such as epoxy, which are typically isotropic and have a low elastic modulus, are used to bond the layers firmly together. The overall material properties of the laminate can be affected by the presence of the adhesive, especially if the laminates are thin and the material properties of the adhesive are dramatically different from those of the individual plies. The effect of a compliant subsurface layer of variable thickness on the contact response of an anisotropic composite half plane is investigated next, where the compliant layer is used to model the presence of the bonding agent. A similar study has been provided by Pindera (1992) for round punch indentation.

Figure 7(a) depicts a layered half plane consisting of a three-ply composite laminate bonded to a homogeneous supporting half plane. The laminate consists of three graphite–epoxy plies, with a stacking sequence of $90°/+45°/-45°$, where the 90° ply is bonded to the $+45°$ ply with a compliant epoxy layer of variable thickness. The thickness of the bond is designated by I, and the thickness of the individual graphite–epoxy plies as h. The

laminate is indented by a rigid flat punch and the resulting separation space is investigated as a function of the thickness l of the compliant layer. Separation parameter spaces are compared for three configurations with distinct compliant layer thickness, zero (non-existent), 20 and 40% of h, designated by l_{00}, l_{20} and l_{40}, respectively. The parameter space consists of two non-dimensional parameters, namely the volume fraction and the ratio of the overall thickness of the surface laminate to the half-width of the punch (H/c).

Figure 7(b) depicts the separation space for the composite half plane for the three case, l_{00}, l_{20} and l_{40}. Of the three cases considered, separation zones generated for the configuration with no compliant layer (designated by the solid line) occupy the greatest amount of area in the parameter space, indicating that there is a greater chance of separation in the absence of a compliant layer. As the thickness of the compliant layer is increased, the separation zones shift to the right and contract along the H/c axis, indicating a reduction in the separation potential due to the reduction in the overall material properties of the surface laminate relative to the underlying half plane.

SUMMARY AND CONCLUSIONS

The effects of off-axis ply orientation, material property mismatch, and the thickness of subsurface compliant layers on the incipient separation phenomenon observed in frictionless flat punch contact problems involving anisotropic layered half planes can be efficiently investigated using the methods outlined in this paper. When a flat punch indents a homogeneous half plane, the contact pressure has a characteristic profile that predicts full contact and exhibits singularities at the corners of the punch. However, deviations in this characteristic profile are observed in layered half planes. The solution predicts complete contact between the punch and the layered structure for only a limited range of geometric and material parameters. Outside this range separation occurs in either one, or two areas of the contact region as discussed by Shield and Bogy for half planes laminated with isotropic layers. The combination of parameters that lead to separation are typically illustrated in a separation parameter space. For isotropic layered half planes, two parameters are employed to describe separation, namely α which describes the ratio of punch half-width to surface layer thickness, and β which describes the elastic modulus mismatch between surface layers and their supporting half plane. In anisotropic layered half planes constructed with fiber-reinforced composite layers, on the other hand, the off-axis orientation and the fiber content of a layer control the through-the-thickness and inplane properties and thus are the relevant parameters to employ in constructing separation spaces.

In this investigation, the parameters α, and v_f were varied in conjunction with off-axis ply orientation in configurations consisting of a single anisotropic layer bonded to a supporting half plane. Separation spaces showing the boundaries between full and two-region, and full and three-region, contact solution zones were presented for 0, 45 and 90° configurations. Varying the orientation of an anisotropic ply changes its resistance to bending and consequently influences the pressure profiles and separation spaces. Due to the orientation of the fibers with respect to the loading plane, a 0° ply has the greatest resistance to bending. Consequently, separation is less likely to occur for a 0° lamina bonded to a supporting half plane. As the ply is rotated through an angle, its resistance to bending is reduced (depending on the degree of anisotropy) and the likelihood of separation is increased.

The effect of a compliant subsurface layer in a $90°/+45°/-45°$ graphite–epoxy laminate bonded to an isotropic half plane was also investigated to demonstrate the ease with which multilayered configurations can be handled with the outlined approach. A separation space was provided that illustrates the effect of varying the thickness of a compliant layer on the boundaries separating full and two-region, and full and three-region, contact solution zones in configurations with different fiber content. The presence of a compliant subsurface layer effectively reduces the overall material properties of a laminate. Thus increasing the thickness of the compliant layer reduces the elastic modulus mismatch between the laminate and the supporting half plane in the direction of the applied load, decreasing the likelihood of separation.

REFERENCES

Aboudi, J. (1991). *Mechanics of Composite Materials: A Unified Micromechanical Approach*. Elsevier, Amsterdam.
Abramowitz, M. and Stegun, I. A. (1965). *Handbook of Mathematical Functions*. Dover.
Binienda, W. K. and Pindera, M.-J. (1994). Frictionless contact of layered metal matrix and polymeric matrix composite half planes. *Compos. Sci. Technol.* **50,** 119–128.
Bufler, H. (1971). Theory of elasticity of a multilayered medium. *J. Elasticity* **1,** 125–143.
Chatterjee, S. N. (1987). Two- and three-dimensional stress fields near delaminations in laminated composite plates. *Int. J. Solids Structures* **23**(11), 1535–1549.
Chatterjee, S. N., Pindera, M.-J., Pipes, R. B. and Dick, B. (1982). Composite Defect Significance. MSC TFR 1312/1108 (NADC Report No. 81034-60), Spring House, PA.
Erdogan, F. (1969). Approximate solutions of systems of singular integral equations. *SIAM J. Appl. Math.* **17**(6), 1041–1059.
Erdogan, F. and Gupta, G. (1972). On the numerical solution of singular integral equations. *Q. J. Appl. Math.* **30,** 525–534.
Gladwell, G. M. L. (1980). *Contact Problems in the Classical Theory of Elasticity*. Sijthoff and Noordhoff, Alphen an den Rijn, The Netherlands.
Pindera, M.-J. (1991). Local/global stiffness matrix formulation for composite materials and structures. *Compos. Engng* **1**(2), 69–83.
Pindera, M.-J. (1992). The effect of a compliant sub-surface layer on frictionless contact of layered half planes. In *Composite Structures and Materials* (Edited by S. V. Hoa and R. Gauvin), pp. 618–626. Elsevier, Amsterdam.
Pindera, M.-J. and Lane, M. S. (1993a). Frictionless contact of layered half planes, part I. Analysis. *J. Appl. Mech.* **60**(3), 633–639.
Pindera, M.-J. and Lane, M. S. (1993b). Frictionless contact of layered half planes, part II. Numerical results. *J. Appl. Mech.* **60**(3), 640–645.
Rowe, R. K. and Booker, J. R. (1982). Finite layer analysis of nonhomogeneous soils. *ASCE J. Engng Mech. Div.* **108**(EM1), 115–132.
Shield, T. W. and Bogy, D. B. (1989). Multiple region contact solutions for a flat indenter on a layered elastic half space: plane strain case. *J. Appl. Mech.* **56,** 251–262.
Urquhart, E. E. (1993). Frictionless Contact of Rigid Indenters on Multilayered Composite Half Planes. Masters Thesis, University of Virginia, Charlottesville, VA.